Research Article | Vol. 27, No. 15 | 22 Jul 2019 | OPTICS EXPRESS 20273
Optics EXPRESS

Solitonic waveguide reflection at an electric interface

M. Alonzo,[1,2] C. Soci,[3] M. Chauvet, [4] and E. Fazio[1,2,*]

[1]Department of Fundamental and Applied Sciences for Engineering, Sapienza Universitá di Roma, Via Scarpa 16, 00161 Roma, Italy
[2]CNIS - Centro di ricerca sulle nanotecnologie applicate all'ingegneria, Sapienza Universitá di Roma, Rome, Italy
[3]Centre for Disruptive Photonic Technologies, Nanyang Technological University, 21 Nanyang Link, 637371 Singapore, Singapore
[4]Department of Optics, FEMTO-ST Institute, UMR CNRS 6174, University of Bourgogne Franche-Comté, 15B avenue des Montboucons, 25030 Besançon, France
*eugenio.fazio@uniroma1.it

Abstract: A refractive index interface is dynamically induced in a bulk photorefractive material by biasing two adjacent regions with different electric fields, thus building up an electric wall. Effects of this interface on reflection, refraction and breathing of bright photorefractive solitons and their associated waveguides are numerically and experimentally studied as a function of the induced purely electric field gradient. Reflection and refraction efficiency depends on the amplitude and sign of the applied voltages that affect both the self-confining beam and the signals propagating inside the waveguide. Experimental tests are performed in nominally undoped lithium niobate samples.

1. Introduction

Dynamically induced self-confined beams and associated waveguides in the bulk of optical media [1, 2] and of photorefractive materials [3–7] have been deeply studied for a long time. They provide the opportunity to overcome the limits of classical guiding structures, because they A) can be generated anywhere in the bulk or on the surface of a host substrate; thus they are real 3D structures; B) the refractive index profile is self-generated leading to optimised waveguides with ultralow propagation losses; C) they are not fixed structures but dynamically addressable. They can be generated and erased depending on the need. Light induced waveguides represent an excellent way to address signals in routing applications, complex processing networks and cognitive photonics.

Different approaches have been tested to control light routing among waveguides [8, 9] or waveguide addressing. For the latter, taking advantage from solitonic interaction that possesses similar properties than colliding quasi-particles, we have the possibility of using mutual repulsion or fusion [10–13] to induce complex waveguides.

Dynamic and effective control of light propagation inside photorefractive materials is still a challenging task. A further step towards the possibility of modifying light paths for local nonlinearities is obtained by forcing radiation to bend in presence of proper refractive index distributions created along propagation paths. In the past a possible solution was achieved by using total reflection of light from crystal physical borders [14] or from interface between two different self-focusing media [15–17]. More recently the possibility of adding electrodes to bend self-confined beams has been investigated both in liquid crystals [18], thanks to their large nonlinearities and in photorefractive materials [24]. An alternative and promising approach takes advantage of intensity modulation inside waveguides to route signals in a stigmergic scheme [19].

Here, we propose to bend, refract or reflect, solitonic beams by switching on proper electric

#360463 https://doi.org/10.1364/OE.27.020273
Journal © 2019 Received 20 Feb 2019; revised 4 May 2019; accepted 6 May 2019; published 9 Jul 2019

Optics EXPRESS

field distributions in the bulk of a photorefractive material by means of external electrodes, so to dynamically create a refractive index interface able to refract or reflect impinging light.

Undoped lithium niobate crystals has been chosen as test photorefractive material because of its well know nonlinearity [4] in pyroelectric configuration [23] in order to free the external surface and make it available for the application of the field generating the interface. However, the proposed procedure is general and can be applied to any photorefractive bulky material.

2. Numerical model and analysis

Spatial soliton formation, propagation, reflection and breathing through a dynamically induced electro-optic interface in the bulk of a nonlinear material is simulated with a robust, custom, FDTD code whose results are in excellent agreement with experimental evidences, as reported also in [19].

One optical field A_1 is propagated with extraordinary polarization in the material perpendicularly to the $\hat{c}$-axis direction. Due to the optical nonlinearity excited by the optical absorption, the A_1 propagation evolves towards a spatial solitonic state, i.e. towards beam self-confinement. A solitonic beam writes a nonlinear refractive index modification. A second beam A_2, at a not-absorbed wavelength, recognizes the solitonic trace written by A_1 as a waveguide and can propagate inside it. A_2 does not excites any nonlinearity and consequently does not modify the solitonic waveguide. Both A_1 and A_2 (at $\lambda_1 = 532nm$ and $\lambda_2 = 787nm$ wavelengths respectively) are shaped as Gaussian beams at the input. The solitonic propagation requires the beam profile to modify into a hyperbolic profile [4]: the profile rearrangement generates losses for both the writing A_1 beam and, in a more evident way, for the propagated A_2 too.

The beam propagations inside the nonlinear medium were simulated by using a FDTD code based on the Helmotz equation written in the form described in Eq. (1) for the generic optical field A_i:

$$\nabla^2 A_i = -\frac{\epsilon_{NL} E_{bias}}{1 + \frac{|A_1|^2}{|A_{sat}|^2}} A_i \tag{1}$$

This equation represents the steady-state propagation of the generic A_i optical beam inside a medium with saturable electro-optic nonlinearity (characterized by its nonlinear dielectric constant ϵ_{NL}) excitable only by the A_1 beam. Thus, A_1 propagates self-confining, while A_2 propagates inside the A_1 channel without modifying it. The electro-optic nonlinearity requires an external static electric bias E_{bias} to generate the photorefractive screening solitons [4]. In this work we have created specific spatial maps of this external bias to induce the electric interface on which A_1 refracts or reflects. In fact, such interface is created via two adjacent but independent electrodes, each of them powered by a proper voltage drop to provide different but uniform bias electric fields parallel to the $\hat{c}$ axis. We refer to these two fields as $E_{bias} = E_i$ and $E_{bias} = E_r$, where the subscripts i and r stand for input and refraction respectively. E_i is the bias field required by the nonlinearity to self-confine the pump optical beam in the input portion of the whole space. E_r is the bias field required by the nonlinearity in the second portion of the space, i.e. after the interface, where the refraction occurs. The continuity of the electric fields across the interface forces the electro-optic effect to generate the refractive index wall on which A_1 reflects and refracts: A_2, propagated inside A_1 channel, will follow the A_1, reflecting or refracting as well.

Effects of the interface on light propagation is analyzed for the light incidence angle $\theta = 0.4°$ with respect to the ideal line defined by electrode borders as in Fig. 1(a).

All simulations are performed in steady state, considering new scenarios for each applied couple of biases. As a general case we report simulations obtained imposing $E_i = 22.5 kV cm^{-1}$ and $E_r = 22.5 \pm 5 kV cm^{-1}$ parallel to E_i for a propagation length $L_z = 10mm$. Electric fields are applied to the pump beam (A_1) focused on the input face of the crystal with a waist of

Optics EXPRESS

$w_0 = 7\mu m$ and having wavelength $\lambda = 532nm$. Considering typical values for refractive index ($n_e = 2.2332$) and electro-optic coefficient ($r_{33} = 32pmV^{-1}$) for extraordinary polarized beams, we obtain a rough estimation for the induced refractive index jump at the interface in the order of $\delta_n = \frac{1}{2} r_{33} n_e^3 E_{bias} \simeq 9 \cdot 10^{-5}$.

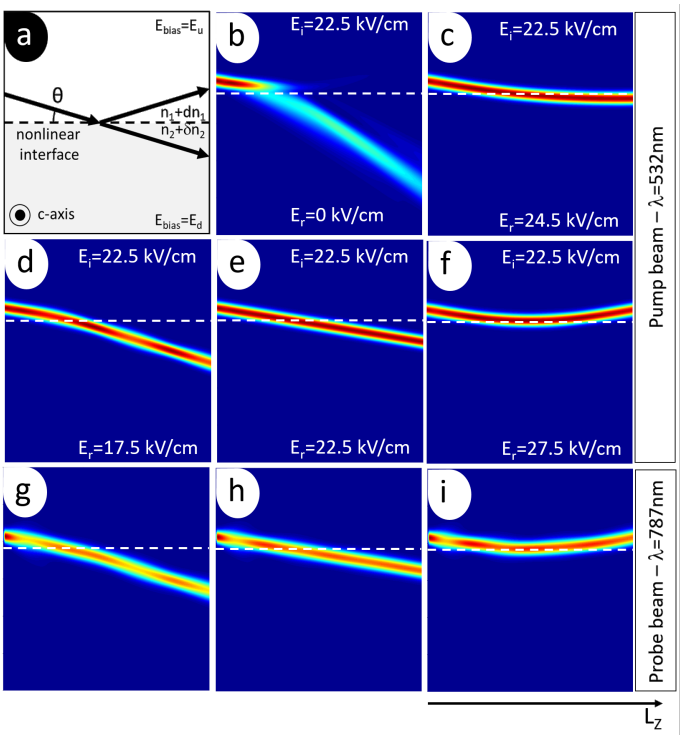

Fig. 1. Effects of the electro-optically-induced interface on spatial soliton propagation. For the pump beam ($\lambda = 532nm$): (a) Scheme of principle in a ray optics approach; (b) Limit refraction condition: the self-confined beam enters a non biased region (below the interface); (c) Critical angle condition for the spatial soliton; (d) Refraction solution for a $E_r = E_i - 5kVcm^{-1}$; (e) Straight spatial soliton propagation: no interface; (f) Spatial soliton reflection for $E_r = E_i + 5kVcm^{-1}$. For the probe beam ($\lambda = 787nm$) propagated inside the written waveguide corresponding to the cases (d)-(e)-(f) respectively: (g) Refraction; (h) No interface; (i) Reflection.

When only the E_i electric field is applied to the whole crystal ($E_r = E_i$), the diffracting pump beam self-confines and reaches the output face of the crystal maintaining the same size all along the propagation path, no matter the angle, Fig. 1(e). In this regime, in absence of any interface, a straight spatial soliton propagates in the bulk following its ideal evolution.

The concept of critical angle, refraction angle which is close to $\pi/2$, is still valid for spatial soliton propagation [24]. Its value is fixed once chosen the E_i and E_r fields. With respect to the critic E_r value, light can be reflected or refracted through the interface by simply increasing or reducing the E_r field. Under the above assumptions, the critical angle associated to the nonlinear propagation of the spatial soliton is obtained for $E_r^{critic} \simeq 24.5kVcm^{-1}$, Fig. 1(c).

The application of the $E_r = 27.5kVcm^{-1}$ electric field causes its reflection, Fig. 1(f) and by reducing E_r to $17.5kVcm^{-1}$ we can drive the interface to refract the beam in the opposite direction, Fig. 1(d).

In presence of $E_r = 0kVcm^{-1}$, Fig. 1(b), the initially self-focused beam is split in a weak reflected contribution and a diffracting, lossy, refracted one by the interface.

Optics EXPRESS

To demonstrate that the interface acts in the same way also for the corresponding waveguide, a probe beam (A_2) is propagated inside the refractive index structure defined by A_1. A_2 is shaped to have the same waist at the input face as the pump beam. Simulations prove that also this wavelength follows exactly the path induced by the pump one, Figs. 1(g)-(i). Some losses are present in correspondence to the first part of the propagation path and a slight breathing appears as well. They can be addressed to the spatial k-vector selection operated by the self-confinement process itself and on the mode mismatch characteristic of the two different wavelengths.

Simulations show also that the electric wall can play a key role in self-confined waveguide breathing. During the process of photorefractive light self-confinement, ideally during the formation of a spatial soliton, the injected beams suffers from an initial strong focusing that selects the proper spatial k-vectors set to be propagated without diffraction. This selection corresponds to the switching from the initial Gaussian transverse mode to a hyperbolic one [4]. In the following we will refer to the position of such strong focusing as to the Gaussian-Hyperbolic (G-H) region. Due to the saturable nature of the involved nonlinearity, this final mode can be thought as the superposition of higher order modes, as demonstrated in [7].

When the interface is activated, both in reflection or in refraction regime, and the beam crosses the self-confined structure, some k-vectors are forced to propagate at larger angles. As photorefractive waveguides exhibit low refractive index contrast with respect to the surrounding material, these k-vectors will propagate outside the induced channel, as propagation losses. By making this crossing closer and closer to the G-H region, the amount of ejected/deviated k-vectors will increase thus modifying the internal mode configuration of the waveguide. This behavior is consistent with the model [20–22] that attributes to the internal mode configuration the origin of waveguide pulsing.

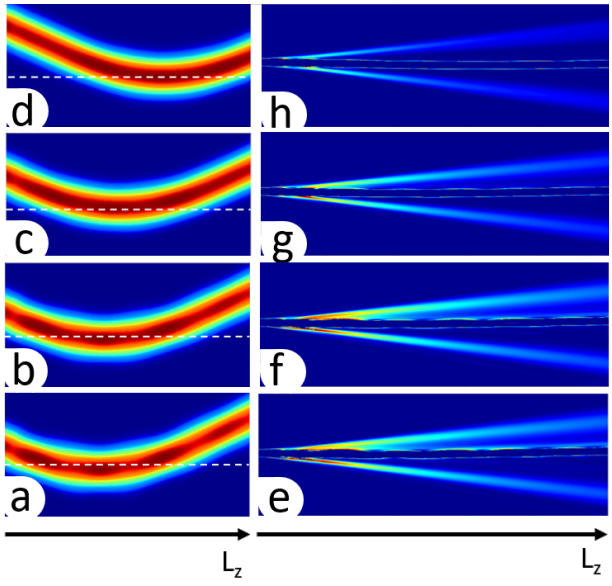

Fig. 2. (a)-(d) Spatial soliton breathing evolution upon reflection by varying the interface crossing distance with the mean G-H position: (a)-(b) breathing. Distances: 2.3 and 2.7mm from the G-H region mean value. (c)-(d) Uniform propagation. Distances: 3.3 and 5mm. (e)-(h) Propagation losses corresponding to the (a)-(d) cases (different visualization scale and images numerically treated): (e)-(f) losses originating from the interface are responsible for breathing; (g)-(h) losses originate mainly from the G-H region and no breathing appears.

Simulations confirms the existence of an high correlation degree between breathing and the

Optics EXPRESS

position of such crossing. Under the same numerical conditions as in Fig. 1, the crossing position between the interface and the waveguide is moved towards the G-H region. Four positions are considered, Figs. 2(a)-(d). Their distances from the mean position of the G-H region are calculated to be about 2.3, 2.7, 3.3 and 5 mm. Moving from the latter position, Fig. 2(d) towards the first one, Fig. 2(a), propagation dynamics changes completely. A uniform propagation switches to a sequence of focusing - defocusing regions, so a breathed evolution.

A further confirmation to this interpretation is found in the analysis of propagation losses. In the two columns figure, Fig. 2, for each of the couples, Figs. 2(d)-(h), Figs. 2(c)-(g), Figs. 2(b)-(f) and Figs. 2(a)-(e) (corresponding respectively to the above four distances), are reported the beam intensity dynamics to emphasize: breathing on the left and the corresponding propagation losses on the right, for the same propagation length L_z. Images on the right, Figs. 2(e)-(h), are obtained by numerically treating Figs. 2(a)-(d) to force to zero any intensity larger than a fixed threshold. This operation makes the waveguide color scale equal to the background leaving only its borders visible. Visualization scale has been adjusted to show losses dynamics up to the last column of the calculation grid. An analysis of Figs. 2(h)-(e) images, show that losses originate mainly in the region where the switching to the hyperbolic profile occurs and that by bringing the crossing position closer to the G-H region, they increase all along the propagation path. This confirms that the interface acts on the waveguide modifying the k-vector distribution base, and thus the internal mode configuration.

Regarding the efficiency of light reflection by the interface, we have investigated the E_r field effects for a fixed incidence angle, 0.4°. In details, simulations calculate the beam centroid position [10] at the output face (c_{out}) of the crystal and compare it with the one at the input (c_{in}) as a function of E_r that is let vary from 0 to $100 kV cm^{-1}$. Defining the quantity $\delta_c = c_{out} - c_{in}$ as the centroid displacement between the output and the input faces, Fig. 3(a) , we find that for $E_r < E_i$ light is refracted below the interface and that the beam is further moved with respect to the expected solitonic position. Above this field threshold value ($E_r = E_i$) for which no interface acts, beam is reflected and beam position at the output face reaches an asymptotic value starting approximately from a field value $E_r \simeq 60 kV cm^{-1}$. In the inset are emphasized the δ_c values corresponding to the E_r field considered in the above discussion.

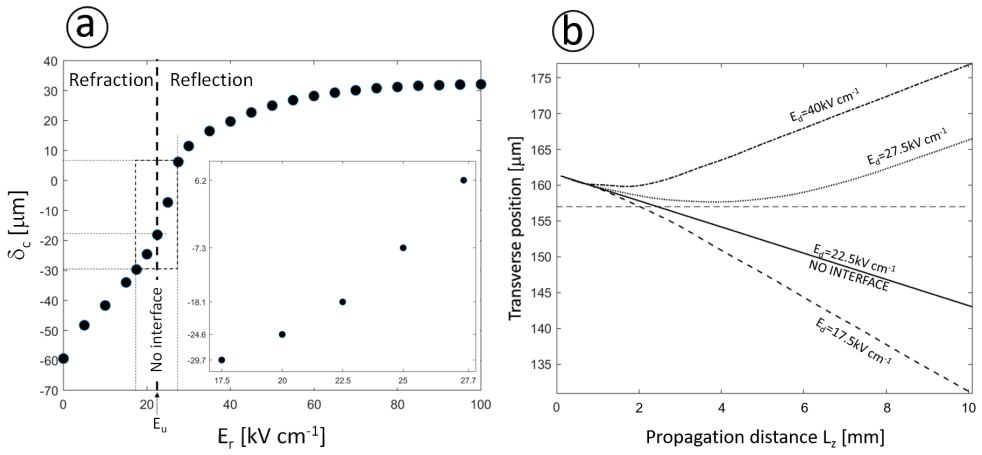

Fig. 3. (a) Beam displacement at the output face with respect to the input position of the calculation grid ($\delta_c = c_{out} - c_{in}$) via a centroid analysis. Inset: detailed values for the cases shown in Fig. 1; (b) Centroid dynamics as a function of the bias electric fields (E_i and E_r) gradient.

Optics EXPRESS

A centroid analysis, Fig. 3(b), reveals that spatial solitons, the quasi-particles, elastically collide with the interface providing a reflection angle equal to the incident one. By increasing the value of the E_r field, so by increasing the refractive index gradient, the reflected beam starts to bend before along the propagation direction and further and further from the interface along the tranverse one. The stronger effect of the interface allows an increased transverse displacement at the output face of the sample and thus an increased addressability of the beam; detailed analysis is discussed in [24].

3. Experiments

The photorefractive material used to test the effect is a congruent, nominally undoped, singledomain Lithium Niobate crystal, nevertheless, the proposed procedure is general and applicable to any photorefractive material.

Besides the many properties that Lithium Niobate owns, it exhibits a strong pyroelectric effect, so the E_i electric field can be induced by heating the sample and for this purpose it is placed on a copper plate connected to a Peltier cell [23] . This local field is generated in the whole volume and directed along the $\hat{c}$-axis. It is made on the order of $E_i \simeq 35 kV cm^{-1}$ by applying a temperature increase $\Delta T \simeq 15°C$, according to the expression $E_{py} = -\frac{1}{\epsilon_0 \epsilon_r} p \Delta T$ and $p \simeq -6 \cdot 10^{-5} Cm^{-2} K^{-1}$ being the pyroelectric coefficient at $25°C$. To apply the E_r field, that must be greater than E_i to achieve reflection, a gold electrode is deposited on a portion of the surface facing the peltier cell (perpendicular to $\hat{c}$) and an external power supply is connected in between this electrode and the copper plate. In this case $E_r = E_{bias} + E_{py}$ being E_{bias} provided by the external power supply. This approach takes into account the different physical nature of the two electric fields. The pyroelectric effect produces a local electric field as the sum of the contributions provided by the unit cell deformation and in turn by the induced dipoles along the $\hat{c}$ axis. The second field, instead, is consequence of the application of a voltage drop across the faces perpendicular to the $\hat{c}$ axis. The latter field requires an external electrical circuit that forces also the temperature induced charges to move thus reducing the pyroelectric contribution effectiveness. By making the self-confinement process faster, for example by increasing the pump beam light intensity, the interface role remains valid. Samples are thinned down to $230 \mu m$ to reduce as much as possible the applied external voltage required to achieve the required E_r field and electrode borders are made as smooth as possible to avoid sharp points for the charged electrical conductor.

Pump and probe beams, with $\lambda_{pump} = 532nm$ and $\lambda_{probe} = 787nm$ respectively, are injected perpendicularly to the $\hat{c}$ axis and propagated to form the desired internal angle with respect to the electrode border in the bulk of the material for a total length of about $6mm$, Fig. 4(k). To achieve a good enough accuracy for the internal incidence angle, the sample is placed on a computer controlled high precision rotation stage. Both beams are shaped with proper optical systems to impinge the surface with a waist in the order of $8 \mu m$. Effects of the dynamically induced electro-optic interface are monitored by using an imaging system able to conjugate with magnification the output face of the sample onto a ccd camera sensor. A detailed analysis of self-confinement dynamics at the output face is possible by the relatively slow Lithium Niobate photorefractive response. In Fig. 4(j), the self-confined solution is compared with the initial diffraction pattern, so the final condition in presence of a bias uniform electric field versus the free propagation regime. Diffraction is approximately circular and has a waist $w_H \simeq w_V \simeq 57 \mu m$. Due to the good optical quality of the used samples and the low scattering, transverse imaging of the propagation paths cannot be performed.

To validate numerical expectations, three sets of measurements are considered and each of them is performed on a different sample to grant propagation paths unaffected by previously induced refractive index modulations. To directly compare evolution dynamics and displacements at the output face of the sample, and to keep the same experimental parameters, each set is realized at different positions along the same vertical direction (parallel to the $\hat{c}$-axis). In Fig. 4

Optics EXPRESS

measurements for an internal angle $\theta_{int} \simeq 0.4°$, $E_i = 35kVcm^{-1}$ and $E_r = E_i \pm 5kVcm^{-1}$ are depicted.

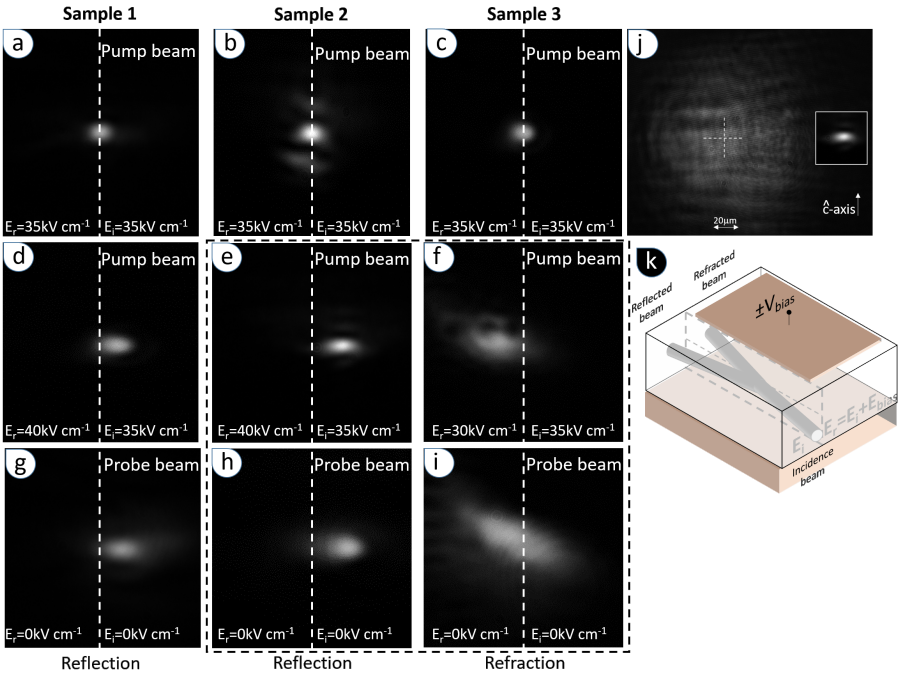

Fig. 4. Experimental evidences of self-confined beam ($\lambda = 532nm$) reflection and refraction in presence of the electro-optical interface (vertical dashed line). Sample 1: breathing free propagation, Sample 2: breathing affected propagation, Sample 3: refraction through the interface. (a),(b),(c) Self-confined beam without interface at the output face of the sample: reference positions. (d),(e),(f) Interface effect when E_r is applied. (g),(h),(i) Induced waveguide probing with the $\lambda = 787nm$ laser line. (k) Scheme of principle.

As numerically predicted, by modulating the distance between the induced interface and the mean G-H region, soliton breathing is expected to become controllable and eventually made negligible by increasing it. Measurements in Sample 1 and Sample 2, respectively Figs. 4(a)-(d) and (g) and Figs. 4(b)-(e) and (h) describe this behavior upon reflection. Firstly, heating is uniformly applied to the sample to achieve self-confinement without any interface and these positions at the output face are taken as reference to evaluate the induced displacements when the interface is switched on, Figs. 4(a)-(b). Then, as a new measurement, a bias contribution is applied to achieve a field $E_r = 40kVcm^{-1}$ that induces the interface. In sample 1, the beam position at the input is shifted $20\mu m$ with respect to sample 2, but the angle is kept the same to increase the distance interface-mean G-H value. Interface action is evident in Figs. 4(d)-(e); in both cases light is reflected with respect to the straight propagation (no interface). Fitting the intensity profile along the $\hat{c}$-axis, a difference is found on the final waist value. In Fig. 4(d) it remains on the order of $w_{out} \simeq 8\mu m$ as at the input face, while in the Fig. 4(e) case it reduces to $w_{out} \simeq 6\mu m$ and a stronger focalisation appears. This is consistent with the beam breathing behavior found numerically. As regards the transverse direction, self-confined beams appear elongated and this can be attributed to different factors, like for example Lithium Niobate anisotropy and inclined propagation with respect to the output face. It is found that the beam centre transverse displacement experienced by the pump beam upon reflection from the interface in sample 2 and 1 is about $\delta_c \simeq 22\mu m$ and $\delta_c \simeq 9\mu m$, Figs. 4(e)-(d) respectively. This different

Optics EXPRESS

behaviour is consequence of the increased interface-mean G-H value distance and thus of the reduced propagation distance for the beam in sample 1. The measurement reported for this case has been realized trying to completely avoid breathing and thus matching the geometrical conditions imposed to achieve the numerical results reported in Fig. 3(a), for which a maximum displacement of $\delta_c \simeq 6.2\mu m$ was found. This difference can be addressed, for example, to a larger electro-optic r_{33} coefficient exhibited by the employed sample.

In sample 3, the E_r field below the gold electrode is decreased to $E_r = 30kV/cm$ by reversing the applied bias voltage. Figs. 4(c)-(f) show respectively the position of the self-confined beam without interface and beam refraction through it. Beam self-focusing is not kept upon refraction and this behavior can be addressed to the fact that by reversing the sign of the E_r contribution, the net field acting on the beam is no more adequate to completely self-confine it, at least in the time during which the pyroelectric field is effective, so until the pyroelectric vanishes due to field screening by charges compensation.

Once the best self-confined solution is obtained, the bias electric fields are switched off and the probe beam is injected collinearly to the pump beam. In the three cases, Figs. 4(g)-(h) and (i), the $787nm$ probe beam feels the induced refractive index variation and propagates following its modulation; at the output face its dimension and position is in excellent agreement with the pump beam one, Figs. 4(d)-(e) and (f). Dynamically induced and bent structure acts also as an efficient waveguide for longer wavelengths. Propagation losses are very low and mainly due to the mode mismatch between the two wavelengths. Furthermore, due to its low energy, this wavelength cannot activate the photorefractive centers and so it can be made propagate without degrade the guide. In the refraction case, a less confined pump beam so a reduced refractive index modulation makes the waveguide still present but less effective, Fig. 4(i).

It is worth noticing that across the interface, beam shape might also be affected by the presence of a border effect due to the difference of the two applied electric fields. For light, distorted electric field lines behave like a cylindrical lens (via the induced distorted refractive index profile), positive or negative according to the electric field gradient, that bends the light mainly along the direction of the $\hat{c}$-axis. This second order effect is expected to remain negligible until when the difference of the two bias field remains small.

4. Conclusion

Efficacy of a purely electrically induced interface in the bulk of a photorefractive material for self-confined waveguide reflection, refraction and breathing control is demonstrated. Numerical simulations and experimental measurements for light beams propagating below the total reflection angle, confirm that a weak refractive index gradient can be used to route a signal transported inside a volumetric and dynamically induced structure. Waveguide deflection can be modulated by changing the amplitude and the sign of the driving electric field E_r with respect to a uniform bias electric field E_i and that upon the reflection regime a saturation value exists.

Furthermore, by making the crossing between the interface and the solitonic waveguide farther to the mean G-H value, waveguide mode distribution is altered thus making breathing minimized or even canceled.

As a consequence, a fully addressable behavior is reached. Such phenomenon allows to formation of curves and complex trajectories within the substrate volume, opening the door to manifold 3D integrated circuits using solitonic waveguides.

Funding

Sapienza Universitá di Roma, grant Progetti di Ricerca - Piccoli (RP116155012228B3-2016).

Optics EXPRESS

Acknowledgments

Authors wish to acknowledge D. Moscatelli for electrode deposition on tested Lithium Niobate samples.

Disclosures

The authors declare that there are no conflicts of interest related to this article.

References

1. R. Y. Chiao, E. Garmire, and C. H. Townes, "Self-trapping of optical beams," Phys. Rev. Lett. **13**(15), 479-482 (1964).
2. V. E. Zakharov, A. B. Shabat, "Exact theory of two-dimensional self-focussing and one-dimensional self-modulating waves in nonlinear media," Sov. Phys. JEPT **34**(1), 62-69 (1972).
3. M. Segev, G. C. Valley, B. Crosignani, P. Di Porto, and A. Yariv, "Steady-state spatial screening solitons in photorefractive materials with external applied field," Phys. Rev. Lett. **73**(24), 3211-3214 (1994).
4. E. Fazio, F. Renzi, R. Rinaldi, M. Bertolotti, M. Chauvet, W. Ramadan, A. Petris, and V. I. Vlad, "Screening-photovoltaic bright solitons in lithium niobate and associated single-mode waveguides," Appl. Phys. Lett. **85**(12), 2193-2195 (2004).
5. M.-F. Shih, Z. Chen, M. Mitchell, M. Segev, H. Lee, R.S. Feigelson., and J.P. Wilde, "Waveguides induced by photorefractive screening solitons," J. Opt. Soc. Am. B **14**(11), 3091-3101 (1997).
6. M. Alonzo, F Pettazzi, M Bazzan, N Argiolas, M V Ciampolillo, S Heidari Batheni, C Sada, D Wolfersberger, A Petris, V I Vlad, and E Fazio, "Self-confined beams in erbium-doped lithium niobate," J. Opt. **12**(11), 015206 (2010).
7. R. Passier, M. Alonzo, and E. Fazio, "Numerical analysis of waveguiding in luminescence-induced spatial soliton channels," IEEE J. Quantum Elect. **48**(11), 1397-1402 (2012).
8. N. Akhmediev, A. Ankiewicz, "Spatial soliton X-junctions and couplers," Opt. Commun. **100**(1-4), 186-192 (1993).
9. J. S. Aitchison, A. Villeneuve, and G. I. Stegeman, "All-optical switching in a nonlinear GaAlAs X junction," Opt. Lett. **18**(14), 1153-1155 (1993).
10. M.R. Belić, A. Stepken, and F. Kaiser, "Spatial screening solitons as particles," Phys. Rev. Lett. **84**(1), 83-86 (2000).
11. Z. Chen, M. Segev, T. H. Coskun, D. N. Christodoulides, and Y. S. Kivshar , "Coupled photorefractive spatial-soliton pairs," J. Opt. Soc. Am. B **14**(11), 3066-3077 (1997).
12. J. S. Aitchison, A. M. Weiner, Y. Silberberg, D. E. Leaird, M. K. Oliver, J. L. Jackel, and P. W. E. Smith, "Experimental observation of spatial soliton interactions," Opt. Lett. **16**(1), 15-17 (1991).
13. M. Alonzo, C. Dan, D. Wolfersberger, and E. Fazio, "Coherent collisions of infrared self-trapped beams in photorefractive InP:Fe," Appl. Phys Lett. **96**(12), 121111 (2010).
14. R. Jager, S.-P. Gorza, C. Cambournac, M. Haelterman, and M. Chauvet, "Sharp waveguide bends induced by spatial solitons," Appl. Phys. Lett. **88**(6), 061117 (2006).
15. E. Alvarado-Méndez, R. Rojas-Laguna, J. G. Aviña-Cervantes, M. Torres-Cisneros, J. A. Andrade-Lucio, J. C. Pedraza-Ortega, E. A. Kuzin, J. J. Sánchez-Mondragón, and V. Vysloukh, "Total internal reflection of spatial solitons at interface formed by a nonlinear saturable and a linear medium," Opt. Commun. **193**(1-6), 267-276 (2001).
16. A. B. Aceves, J. V. Moloney, and A. C. Newell,"Theory of light-beam propagation at nonlinear interfaces. I. Equivalent-particle theory for a single interface," Phys. Rev. A **39**(4), 1809-1827 (1989).
17. L. Jankovic, H. Kim, G. Stegeman, S. Carrasco, L. Torner, and M. Katz,"Quadratic soliton self-reflection at a quadratically nonlinear interface," Opt. Lett **28**(21), 2103-2105 (2003).
18. M. Peccianti, A Dyadyusha, M. Kaczmarek, and G. Assanto, "Tunable refraction and reflection of self-confined light beams," Nat. Phys. **2**(11), 737-742 (2006).
19. M. Alonzo, D. Moscatelli, L. Bastiani, A. Belardini, C. Soci and E. Fazio, "All-optical reinforcement learning in solitonic x-junctions," Sci. Rep. **8**(1), 5716 (2018).
20. I. Shadrivov, A. A. Zharov,"Interaction of vector solitons with a nonlinear interface," Opt. Comm. **216**(1-3), 47-54 (2003).
21. Y. S. Kivshar, D. E. Pelinovsky, T. Cretegny, and M. Peyrard,"Internal modes of solitary waves," Phys. Rev. Lett. **80**(23), 5032-5035 (1998).
22. C. Etrich, U. Peschel, F. Lederer, B. A. Malomed, and Y. S. Kivshar, "Origin of the persistent oscillations of solitary waves in nonlinear quadratic media," Phys. Rev. E **54**(4), 4321-4324 (1996).
23. J. Safioui, F. Devaux, and M. Chauvet, "Pyroliton: pyroelectric spatial soliton," Opt. Lett. **17**(24), 22209-22216 (2009).
24. E. Fazio, M. Alonzo, and A. Belardini, "Addressable refraction and curved soliton waveguides using electric interfaces," Appl. Sci. **9**(2), 347 (2019).